# Validation and investigation of reactive species yields of Geant4- DNA chemistry models

Dylan Peukert, Sebastien Incerti, Ivan Kempson, Michael Douglass, Mathieu Karamitros, Gérard Baldacchino, Eva Bezak

# Validation and investigation of reactive species yields of Geant4-DNA chemistry models

Dylan Peukert
*Future Industries Institute, University of South Australia, Adelaide, SA, Australia*
*Division of ITEE, University of South Australia, Adelaide, SA, Australia*

Sebastien Incerti
*Univ. Bordeaux CENBG UMR 5797, Gradignan F-33170, France*
*CNRS IN2P3 CENBG UMR 5797, Gradignan F-33170, France*

Ivan Kempson
*Future Industries Institute, University of South Australia, Adelaide, SA, Australia*

Michael Douglass
*Department of Medical Physics, Royal Adelaide Hospital, Adelaide, SA, Australia*
*Department of Physics, University of Adelaide, Adelaide, SA, Australia*

Mathieu Karamitros
*Radiation Laboratory University of Notre Dame, Notre Dame, IN46556, USA*

Gérard Baldacchino
*LIDYL UMR 9222 CEA-CNRS-Université Paris-Saclay CEA Paris-Saclay, F-91191 Gif sur Yvette, France*

Eva Bezak[a)]
*Department of Physics, University of Adelaide, Adelaide, SA, Australia*
*Cancer Research Institute and School of Health Sciences, University of South Australia, Adelaide, SA, Australia*

(Received 6 August 2018; revised 22 November 2018; accepted for publication 2 December 2018; published 26 December 2018)

**Purpose:** Indirect biological damage due to reactive species produced in water radiolysis reactions is responsible for the majority of biological effect for low linear energy transfer (LET) radiation. Modeling water radiolysis and the subsequent interactions of reactive species, as well as track structures, is essential to model radiobiology on the microscale. Recently, chemistry models have been developed for Geant4-DNA to be used in combination with the comprehensive existing physics models. In the current work, the first detailed, independent, in silico validation of all species yields with published experimental observations and comparison with other radiobiological simulations is presented. Additionally, the effect of LET of protons and heavier ions on reactive species yield in the model was examined, as well as the completeness of the chemical reactions following the radiolysis within the time after physical interactions simulated in the model.
**Methods:** Yields over time of reactive species were simulated for water radiolysis by incident electrons, protons, alpha particles, and ions with various LETs using Geant4 and RITRACKS simulation tools. Water dissociation and recombination was simulated using Geant4 to determine the completeness of chemical reactions at the end of the simulation. Yield validation was performed by comparing yields simulated using Geant4 with experimental observations and other simulations. Validation was performed for all species for low LET radiation and the solvated electron and hydroxyl radical for high LET ions.
**Results:** It was found that the Geant4-DNA chemistry yields were generally in good agreement with experimental observations and other simulations. However, the Geant4-DNA yields for the hydroxyl radical and hydrogen peroxide at the end of the chemistry stage were found to be respectively considerably higher and lower than the experimentally observed yields. Increasing the LET of incident hadrons increased the yield of secondary species and decreased the yield of primary species. The effect of LET on the yield of the hydroxyl radical at 100 ns simulated with Geant4 was in good agreement with experimental measurements. Additionally, by the end of the simulation only 40% of dissociated water molecules had been recombined and the rate of recombination was slowing.
**Conclusions:** The yields simulated using Geant4 are within reasonable agreement with experimental observations. Higher LET radiation corresponds with increased yields of secondary species and decreased yields of primary species. These trends combined with the LET having similar effects on the 100 ns hydroxyl radical yield for Geant4 and experimental measurements indicate that Geant4 accurately models the effect of LET on radiolysis yields. The limited recombination within the modeled chemistry stage and the slowing rate of recombination at the end of the stage indicate potential

long-range indirect biological damage. 
[https://doi.org/10.1002/mp.13332]

Key words: model validation, Monte Carlo, radiation chemistry, radiobiology, water radiolysis

## 1. INTRODUCTION

Radiation therapy is used in the treatment of cancer for a large proportion of patients. Studies have shown that for radiation types with a low LET such as photons and protons, the majority of the biological effect is caused by indirect chemical damage via radicals and reactive species produced by water radiolysis as water is the primary constituent of most living organisms.[1] These species include reactive oxygen species (ROS) which mainly cause oxidative reactions contributing to oxidative stress. These ROS are the hydroxyl radical ($^{\bullet}OH$), hydrogen peroxide ($H_2O_2$), and the superoxide radical ($O_2^{\bullet-}$).[2] The remaining contribution to the biological effect is the result of direct physical damage from ionization of atoms in biological targets.[3] To comprehensively model radiobiology on the microscale, it is necessary to model both the track structure of the incident particles, the resulting water radiolysis, and the 3D distribution of reactive species over time.[4,5] As such, it is necessary to model the diffusion, reactions, and recombination of the reactive species produced by the radiolysis.[6] The modeling of the production, diffusion reactions, and recombination of numerous reactive species over time following physical interactions are computationally intensive, as such, most simulations of radiobiological effects consider only the physical dose and direct damage with appropriate scaling. While this is sufficient for modeling many macroscale radiobiological effects, there are cases where modeling the direct damage alone cannot explain experimental observations. For example, there are indications that ROS play a major role in the enhancement of proton radiotherapy by high Z metallic nanoparticles.[7–11]

Geant4[12,13] is an open source Monte Carlo simulation toolkit with a comprehensive library of physics models for a wide variety of particles and energies. Additionally, Geant4 has the capability to model intricate simulation geometries that can consist of complex shapes made of many elements, isotopes, materials, and molecules. The Geant4-DNA[14,15] very low energy physics models allow modeling of the microscale track structures for directly ionizing radiation in water via discrete step-by-step interactions and have been used extensively in radiobiological modeling. The addition of chemistry modeling to Geant4-DNA[16,17] allows the modeling of the production, diffusion, reactions, and recombination of reactive species resulting from water radiolysis. The chemistry models of Geant4-DNA provide new tools to the user extending the possible applications for the toolkit that can be further developed by users. One such potential new application of the models could be complete radiobiological modeling taking into account the physical, chemical, and biological stages of radiobiology, resolving the gap between the physical and biological stages present in many radiobiological models.

While there are several simulation tools capable of modeling radiolysis available, the majority model the chemical stage using independent reaction time (IRT) methods.[18–21] IRT simulations provide a computationally efficient and accurate simulation of radiolysis yields; however, they do not track the diffusion jumps of individual reactive species over time during the chemical stage as required for radiobiological modeling.[22] Of the few remaining models that can provide this level of information, Geant4-DNA chemistry is advantageous due to Geant4's comprehensive physics models for many particles and the ability to have complex geometries consisting of many materials. Geant4, and tools built upon it such as GATE[23] and TOPAS,[24] is already widely used in radiobiological modeling. As such, the addition of chemistry models in Geant4 provides a convenient pathway to the incorporation of the chemical stage of radiation damage in radiobiological models. Further, the open source nature of Geant4 allows for comprehensive modification of all simulation aspects, the possibility of replication of simulations, as well as collaboration and sharing of simulation code.

Validation of a newly developed model is essential to provide confidence in simulation results, to quantify the accuracy of the simulation and to understand the limitations of the model. In the validation of a model, the results of simulations are compared to experimental measurements to test the model's accuracy.

The radiation chemistry models in Geant4-DNA were developed for applications in radiobiological modeling. As such, the chemistry tracking is limited to water under typical biological conditions of temperature of 37°C and pH 6–7. For validation, the Geant4-DNA physics and chemistry models were used to simulate water radiolysis and the yield of reactive species G (species/100 eV energy deposition) was calculated over times from 1 ps to 1 μs and compared with experimental measurements taken for pure water at room temperature (the closest conditions to those in biology for which measurements were available). Measurements taken for nonwater radiolysis and water radiolysis in nonbiological conditions such as extreme temperature, pressure, or pH were excluded in this work. However, users can adapt their own parameter set for other conditions using available data bases.[25,26]

Geant4-DNA chemistry models have not had a published comprehensive, independent validation against experimental measurements. This is shown by the review of papers using Geant4-DNA chemistry in Section 3. In view of this, and the great potential utility of these radiation chemistry models, a comprehensive validation of the chemical yields predicted by Geant4-DNA chemistry against experimental measurements and a comparison to

other radiation chemistry simulation tools were performed and presented for the first time in this article. Additionally, an investigation was also performed into other characteristics of the simulation, such as the effect of particle type and LET on the chemical yields over time, and the completeness of chemical interactions at the end of the 1 μs period after the physical interactions are simulated.

Section 2 provides a brief overview of the Geant4-DNA radiation chemistry modeling encompassing the physical, physicochemical, and chemical stages of the simulation. Section 3 is a comprehensive review of publications that use Geant4-DNA chemistry simulations. Section 4 provides a description of the simulation geometry and irradiation setup used in the simulation, as well the simulations and relevant analyses performed. Section 5 presents the simulation results for the validation of Geant4-DNA chemical yields with experimental measurements and comparison with other radiation chemistry models, the effect of LET and particle type on the chemical yields over time and the completeness of the chemical reactions when the chemistry simulation ceases. A discussion of experimental results is presented in Section 6. An overall conclusion is presented in Section 7.

## 2. OVERVIEW OF GEANT4-DNA WATER RADIOLYSIS MODELING

The most recent public release of Geant4, version 10.4 (December 2017), provides Geant4-DNA users with a full set of physical, physicochemical, and chemical models and processes for the modeling of water radiolysis induced by ionizing particles in liquid water, up to one microsecond after irradiation. We present a brief overview of these processes below and in Fig. 1 with detailed information about the models and their development provided in relevant cited papers detailing recent advances in radiation chemistry.[27]

### 2.A. Physical processes

Geant4-DNA can simulate track structures of ionizing radiation in liquid water thanks to a variety of discrete processes describing step-by-step physical interactions, during the so-called "physical stage" of water radiolysis. The physical interactions of electrons, protons and neutral hydrogen atoms, alpha particles, and their charged states, as well as a selection of heavier ions dominant in the cosmic spectrum,

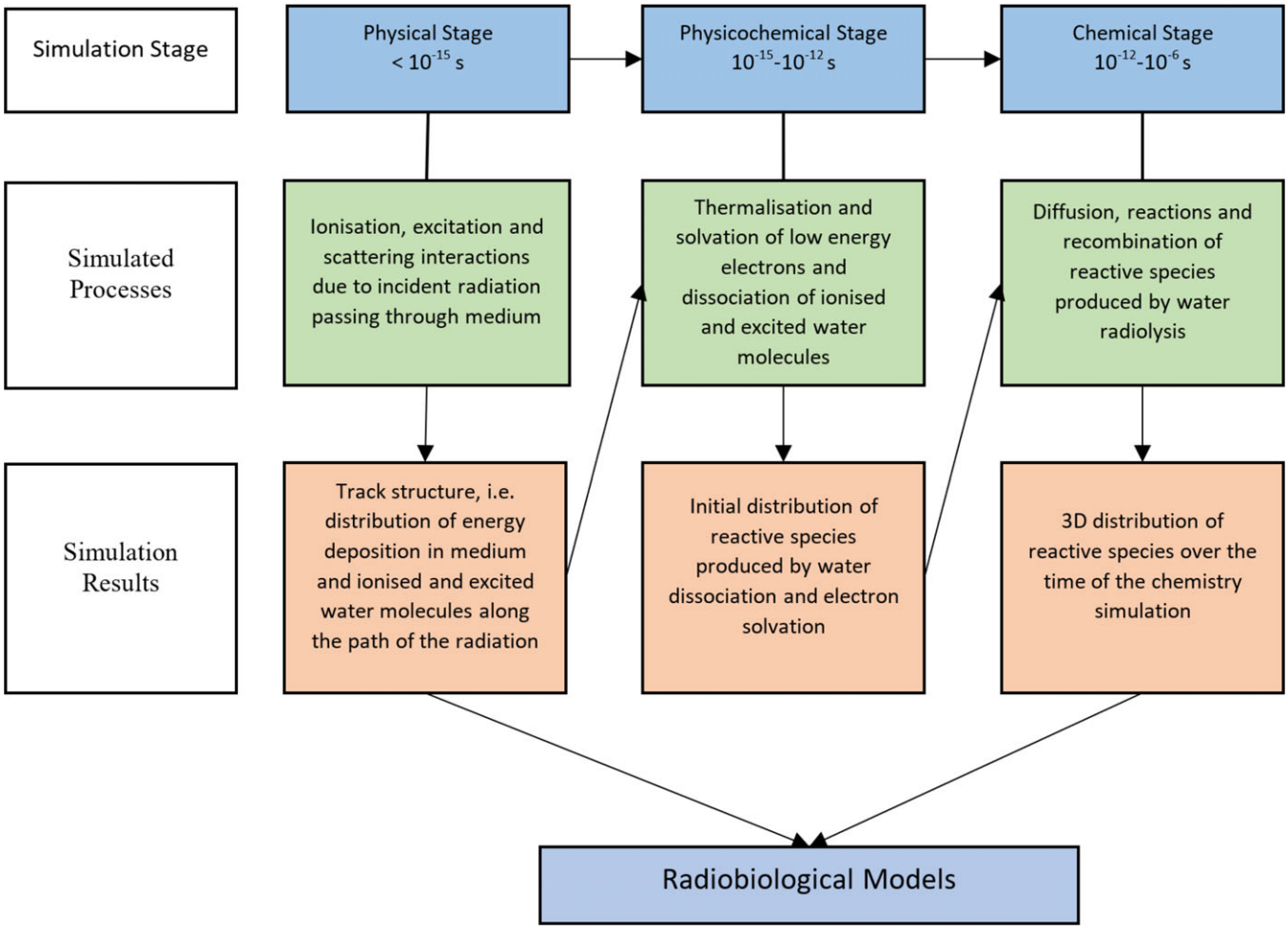


FIG. 1. Flowchart providing an overview of the physical, physicochemical, and chemical stages of the Geant4-DNA simulation showing the outputs that can be exported to radiobiological models. [Color figure can be viewed at wileyonlinelibrary.com]

(Lithium-7, Beryllium-9, Boron-11, Carbon-12, Nitrogen-14, Oxygen-16, Silicon-28, Iron-56) are available. They include elastic scattering, ionization, electronic excitation, and charge exchange processes. For the heavier ions, only the ionization process is considered taking into account an effective charge scaling. These physical processes use dedicated models to describe fully the physical interaction (that is, the calculation of cross section and the description of the interaction final state, such as energy loss, angular deviation, and production of secondary particles). For most physical processes, several alternative models are available. In order to facilitate their usage, such models and processes are assembled into "physics constructors". The models available for the description of electron interactions are gathered into three alternative physics constructors, which can also describe the interactions of protons, neutral hydrogen atoms, alpha particles, their charged states, and the heavier ions using the same set of models. These constructors are named as "G4EmDNA Physics_option2", "G4EmDNAPhysics_option4", and "G4 EmDNAPhysics_option6". These processes and models have been already extensively described in the literature (see Ref. [14,15,28–30] and cited references therein).

In brief, the "G4EmDNAPhysics_option2" constructor contains the default models initially used in Geant4-DNA: inelastic interactions for electrons are computed from the dielectric response function formalism and elastic interactions are based on a partial wave analysis. This constructor also includes subexcitation processes such as vibrational excitation and molecular attachment for electrons derived from experimental measurements. The "G4EmDNAPhysics_option4" includes an improved version of the inelastic models based on the dielectric response function developed at Ioannina University in Greece, as well as an improved version of the screened Rutherford elastic model for electrons. Finally, the recent "G4EmDNAPhysics_option6" constructor proposes an independent set of models of electrons, initially available from the well-known CPA100 track structure code developed at Paul Sabatier University in Toulouse, France[31]; in particular it uses the Binary-Encounter-Bethe approach for the modeling of ionization and the independent atom method for the modeling of elastic interactions. The default models were used in this work due to a greater coverage of energies (up to 1 MeV) for electrons.

The physical stage proceeds until the physical processes of the primary particles and all secondary particles are modeled. The modeling of physical processes of a particle can stop for three potential reasons. The modeling of a particle can be ceased by user command, alternatively, the particle's processes are modeled until either the particle stops in the simulation volume or leaves the simulation volume. When the chemistry model is activated, electrons are not modeled until they stop within the simulation volume, instead, electrons are modeled until an energy of 7.4 eV is reached and they are then passed to the next stage of the simulation. The distribution of ionized and excited water molecules and subexcitation electrons are passed to the physicochemical stage of the simulation.

## 2.B. Physicochemical processes

The physicochemical processes of Geant4-DNA take place during the "physicochemical" stage of water radiolysis, from a few femtoseconds up to a few picoseconds after the physical stage. During this stage, subexcitation electrons thermalize down to 25 meV and become solvated. The thermalization process offers two alternative approaches. The first approach tracks the electron down to 25 meV using all step-by-step Geant4-DNA processes available in this energy range. The second approach simulates the thermalization by displacing the electron in a single step once the electron has reached a predetermined energy, avoiding multiple, time consuming, simulation steps. Due to the lack of reliability of the models in this energy range (25 meV–10 eV), the accuracy of the step-by-step approach is not guaranteed. Nevertheless, because the dissociative attachment process is defined down to 4 eV, choosing one or the other of the approaches may impact the initial number of hydroxyl radicals and solvated electrons. The single-step approach offers three alternative thermalization models. The first two models are described in earlier publications and use step-by-step track structure Monte Carlo simulations of electron transport down to sub eV energies.[31,32] The third model uses a mean penetration length proportional to the initial kinetic energy of the electron before thermalization. By default, the proportionality constant is taken as 1.8 nm/eV following Ritchie et al.[33] The default thermalization process uses the single-step approach as detailed by Bernal et al.[15] In addition, ionized or excited water molecules undergo modifications of their electronic configuration which can lead to radiative and/or dissociative rearrangement. The dissociation scheme used in Geant4-DNA follows the initial approach of the PARTRAC state-of-the-art Monte Carlo code for biological damage modeling[34] and is given in Table I. This table is implemented in a dedicated "chemistry constructor", named "G4EmDNAChemistry". However, the user can implement their own custom dissociation scheme.

In addition to these rearrangements, a specific process ("G4DNAWaterDissociationDisplacer") is responsible for the placement of the dissociation products, including a specific parameterization for solvated electrons. All parameters used for the placement of these dissociation products are described by Bernal et al.[15] The physicochemical stage is complete once all subexcitation electrons are solvated and all excited or ionized water molecules dissociate. These processes provide the initial distribution of reactive species that is used in the chemistry stage of the simulation.

## 2.C. Chemical processes

After the "physicochemical" stage, Geant4-DNA chemical processes can simulate step-by-step the Brownian diffusion of molecular species up to one microsecond after irradiation using the Smoluchowski model.[17] Geant4-DNA follows a particle-based approach for the simulation of water

TABLE I. Dissociation schemes used in Geant4-DNA version 10.4 (December 2017). AI stands for Auto-Ionization. This table is recalled from Ref. [15] and it is implemented in the G4EmDNAChemistry chemistry constructor.

| Electronic state of water Molecule | Dissociation channels | Fraction (%) |
|---|---|---|
| All single ionization states: $H_2O^+$ | $H_3O^+ + {}^{\bullet}OH$ | 100 |
| Excitation state A1B1: | ${}^{\bullet}OH + H^{\bullet}$ | 65 |
| (1b1) → (4a1/3s) | $H_2O + \Delta E$ | 35 |
| Excitation state B1A1: | $H_3O^+ + {}^{\bullet}OH + e^-_{aq}$ (AI) | 55 |
| (3a1) → (4a1/3s) | ${}^{\bullet}OH + {}^{\bullet}OH + H_2$ | 15 |
| | $H_2O + \Delta E$ | 30 |
| Excitation state: | $H_3O^+ + {}^{\bullet}OH + e^-_{aq}$ (AI) | 50 |
| Rydberg, diffusion bands | $H_2O + \Delta E$ | 50 |
| Dissociative attachment: $H_2O^-$ | ${}^{\bullet}OH + OH^- + H_2$ | 100 |

TABLE II. Molecular species and their diffusion coefficient available in Geant4 10.4 (December 2017).

| Molecular species | Diffusion coefficient ($10^{-9}$ $m^2$ $s^{-1}$) |
|---|---|
| $e^-_{aq}$ | 4.9 |
| ${}^{\bullet}OH$ | 2.8 |
| $H^{\bullet}$ | 7.0 |
| $H_3O^+$ | 9.0 |
| $H_2$ | 5.0 |
| $OH^-$ | 5.0 |
| $H_2O_2$ | 1.4 |

radiolysis,[15–17] where species are modeled as point-like objects diffusing in a continuous liquid water medium. The chemical reactions are diffusion-controlled, which means that a reaction can happen between two reactants as soon as their separation distance is less than a reaction radius calculated from the reaction rate. The Geant4-DNA chemistry simulation uses dynamically computed time steps. In order to speed up the simulations, a minimum time step can be selected by the user in order to prevent too short time steps leading to prohibitive simulation times. When the computed time step is shorter than the user defined minimum time step, Geant4-DNA uses a Brownian bridge process to account for possible encounters between reactants during the minimum time step. The Brownian Bridge process is described in detail by Karamitros et al.[17] The list of species handled by Geant4-DNA in Geant4 release 10.4 is given in Table II and their corresponding chemical reactions are shown in Table III.

All parameters listed in Tables I–III can be modified by the user. The modeling of radiolysis is currently up to one microsecond; this is the time limit adopted by Monte Carlo codes beyond which heterogeneous chemical interactions within a track cease and homogeneous interactions begin as the reactive species diffuse away from the track.[35] The limit is also used as beyond 1 μs biological repair processes start to be active when simulating biological damage from ionizing radiation.

## 3. REVIEW OF GEANT4-DNA-BASED WATER RADIOLYSIS SIMULATIONS

Most Geant4-DNA research focuses exclusively on the simulation of track structures in liquid water, as reviewed in Ref. [36] At the time of publication, there are few published works based on the simulation of water radiolysis using the recently developed Geant4-DNA chemistry model.

Abolfath et al.[37] were the first to use Geant4-DNA for the simulation of ionizations along track structures of 1 MeV electrons and protons in combination with molecular dynamic simulations (ReaxFF environment), in order to model the radiolysis and resulting DNA-•OH chemical reactions for the prediction of DNA damage.

Pachnerova Brabcova et al.[38] then presented the first experimental validation of Geant4-DNA water radiolysis. Irradiating pBR322 plasmids with 30 MeV protons in liquid water and in the presence of coumarin-3-carboxylic acid (a hydroxyl scavenger), they could measure radiochemical yields of •OH radicals as a function of time based on fluorescence measurements of the hydroxylated form (7-hydroxy-coumarin-3-carboxylic acid) using a method described elsewhere.[39–41] Although they could not simulate water radiolysis in the whole irradiated volume, they simulated 20 MeV proton tracks traversing a 5 μm cube of liquid water. They concluded that the simulated •OH radical yields in time were in acceptable agreement with the experimental data, observing that radical yields sharply decrease in time due to reactions with scavengers and other radical species, up to 1 μs.

In the context of the investigation of radiation damage to the central nervous system, Belov et al.[42] simulated early biological damage induced by ionizing radiation using Geant4-DNA in a sample neural network as the target. They simulated water radiolysis from proton, carbon-12, and iron-56 irradiation within a wide range of linear energy transfer values (from a few to hundreds of keV/μm). They simulated radiochemical yields and absolute yields of molecular species (which depend on geometrical properties of the simulated target) as a function of time, as well as mean numbers of species as a function of LET at different times. They underlined the

TABLE III. Chemical reactions and their reaction rate available in Geant4 10.4 (December 2017) and implemented in the G4EmDNAChemistry chemistry constructor.

| Reaction | Reaction rate ($10^7$ $m^3$ $mol^{-1}$ $s^{-1}$) |
|---|---|
| $H^{\bullet} + e^-_{aq} + H_2O \rightarrow OH^- + H_2$ | 2.65 |
| $H^{\bullet} + {}^{\bullet}OH \rightarrow H_2O$ | 1.44 |
| $H^{\bullet} + H^{\bullet} \rightarrow H_2$ | 1.20 |
| $H_2O_2 + e^-_{aq} \rightarrow OH^- + {}^{\bullet}OH$ | 1.41 |
| $H_3O^+ + e^-_{aq} \rightarrow H^{\bullet} + H_2O$ | 2.11 |
| $H_3O^+ + OH^- \rightarrow 2\,H_2O$ | 14.3 |
| ${}^{\bullet}OH + e^-_{aq} \rightarrow OH^-$ | 2.95 |
| ${}^{\bullet}OH + {}^{\bullet}OH \rightarrow H_2O_2$ | 0.44 |
| $e^-_{aq} + e^-_{aq} + 2\,H_2O \rightarrow 2\,OH^- + H_2$ | 0.50 |

influence of the network geometry on the production of radiolysis products and suggested that the observed enhancement in the levels of ROS may potentially lead to oxidative damage to neuronal components disrupting the normal communication between cells of the neural network.

Tran et al.[10] investigated the production of molecular species around gold nanoparticles (GNP) using Geant4-DNA. GNPs are currently being studied as potential candidates for increasing the effectiveness of radiotherapy treatments. The nanoparticles were irradiated with 2–170 MeV protons. In particular, the authors presented the time evolution of the one-dimensional distribution of chemical species around the GNP as a function of radial distance and the radiolysis enhancement factor as a function of this distance (compared to liquid water only). They underlined the similar trends between the simulated radiolysis enhancement factors and the absorbed dose enhancement factors around the GNP.

Finally, Tian et al.[43] recently developed a new graphics processing unit (GPU)-based simulation platform adapted from Geant4-DNA which allows accelerated computing times (up to 200× faster) for the simulation of water radiolysis. In their study, Tian et al. also compared radiolytic yields over time simulated using Geant4-DNA with PARTRAC simulations[34] for 750 keV electrons and 5 MeV protons. Differences in the yields of hydroxyl radical and solvated electrons were observed. However, as the chemistry models used were altered, the yields are not representative of the default Geant4-DNA chemistry models.

All these Geant4-DNA-based simulations present the first original applications of Geant4-DNA water radiolysis. However, so far, none of them have addressed in detail and quantitatively the performance and accuracy of Geant4-DNA for water radiolysis modeling. The main objective of this work is thus to present for the first time a detailed evaluation of Geant4-DNA water radiolysis modeling capabilities, by comparing Geant4-DNA simulations to a collection of experimental data in liquid water and to other Monte Carlo simulations.

## 4. MATERIALS AND METHODS

### 4.A. Simulation geometry and irradiation conditions

The simulation geometry consisted of a 10 m × 10 m × 10 m water cube. A large volume was chosen to ensure that all secondary particles and the produced reactive species did not leave the simulation volume. Irradiation was performed using a monoenergetic pencil beam in the positive Z direction which originated in the center of the water cube. Irradiations with primary particles of 1 and 50 MeV protons, 1 and 5 MeV alpha particles, 1 MeV electrons, 1.14 and 4.8 GeV carbon-12 ions, and 1.34 and 5.285 GeV silicon-28 ions were simulated. For each particle type and energy, $10^5$ primary particles were simulated. Tracking of the primary particles ceased after the primary particles had lost 1 keV of energy for lower LET primary particles, 2 keV for 1 MeV alpha particles and 5.285 GeV silicon ions and 5 keV for 1.34 GeV silicon ions. The energy cutoffs were chosen to ensure that the simulated tracks had a length equal to or greater than 20 nm. Sensitivity testing showed that this requirement was sufficient to ensure that there were no measurable track end effects on the yield. The cessation of primary particle tracking was done to ensure that the simulation provided results of a section of the beam with a fixed LET value (Track segment LET), allowing the quantification of the effect of the primary particles' LET on reactive species production. Additionally, this reduced the computation time per event of the simulation allowing a greater number of events to be simulated with an improvement in the resulting statistics.

The total energy lost by all particles in the simulation was also tracked. Events in the simulation were aborted if the total cumulative energy loss was greater than 8 keV for lower LET primary particles, 16 keV for 1 MeV alpha particles and 5.285 GeV silicon ions and 40 keV for 1.34 GeV silicon ions. This was done to remove events in the simulation where the primary particles deposit considerably more energy than the cutoff. There are several ways that this can occur. The primary particle's type can be changed via charge exchange resulting in the tracking of energy lost by the primary particle to cease. Alternatively, the primary particle can deposit its entire energy in a single interaction. As the energy loss is calculated by querying the particles' energy after the simulation step, if the particle is removed from the simulation in an interaction the energy loss is not considered. In these scenarios, tracking only the primary particle's energy loss is insufficient to cease tracking the primary particle after energy deposition on the order of the cutoff limit. These events are aborted as their simulation times are several orders of magnitude greater than normal and eventually they congest all threads of the simulation causing a large increase in the average time per event of the simulation.

The simulation records the total energy deposited, as well as the number of reactive species generated, in the water volume via radiolysis. The yield of each of the seven species simulated in Geant4-DNA chemistry is recorded separately. The energy deposited, and the number of species are recorded at time points in the chemistry simulation stage ranging from 0.5 ps to 1 μs after the start of physical interactions. The time points have a logarithmic distribution given the time scales involved span multiple orders of magnitude. For studies of the completeness of the reactive species' reactions within the simulated chemistry stage, two pseudo-species which do not diffuse or interact are also tracked. These pseudo-species represent the dissociation and recombination of water molecules in the simulation.

For comparison, reactive species' yield simulations were also performed using the RITRACKS (Version 3.1) simulation software.[44,45] In these simulations, the irradiation beam geometry is the same as for the Geant4 simulations. The RITRACKS simulations occur in an unbounded water phantom. In the RITRACKS simulations, the number of reactive species and energy deposited are recorded for time points

with logarithmic distribution between 1 fs and 1 μs. In the RITRACKS simulations, the tracking of the primary particle in the simulation was stopped after the particle had traveled a distance corresponding to the mean path length for the particle to deposit 1–5 keV of energy as found from the LET within the simulation. Testing the Geant4 simulation using this method showed no difference in results compared to ceasing tracking based on energy deposition.

### 4.B. Analysis

The yield for each reactive species was normalized to be independent of the energy deposited by calculating the yield G, the number of molecules of a species generated per 100 eV of energy deposited. This normalized yield was used in all cases except for the study of the completeness of the chemistry simulation, in which case the yield was measured in terms of molecules per primary particle.

For the yield verification, the reactive species' yields simulated using Geant4-DNA chemistry models were compared with experimental measurements available for validation, as well as the results of other radiation chemistry simulations. Comparisons were performed for low LET radiation types such as fast electrons, gamma rays, and high energy protons, as these were used in the majority of experimental observations. The Geant4 simulations were performed using a monoenergetic 1 MeV (0.999 MeV) electron beam, as this was the highest energy for which the most accurate Geant4-DNA physics models were available for electrons. Geant4 and RITRACKS simulations were performed for this validation, while PARTRAC[46] simulation results and experimental observations were taken from the literature. When comparing radiolysis simulations, note that both changes in the physics and chemistry models used can result in differences in the reactive species' yields, a comparison of the Geant4-DNA and RITRACKS physics models was performed by Douglass et al.[47] Experimental measurements of time-dependent yields were available for use in validation for all species modeled in Geant4 except the hydrogen radical and the hydroxyl ion while measurements of the primary yields were available for all species except the hydroxyl ion. The primary yield is the yield when heterogeneous chemical interactions within the track end and homogenous chemical reactions begin.[35,48]

Validation of higher LET radiation types such as ions was also performed. Due to limited experimental measurements where the G-values are determined in a short range of track segment LET conditions, the high LET validation was performed for only the solvated electron and hydroxyl radical for carbon and argon ions. The yields from the Geant4 simulation were compared with RITRACKS yields and experimental observations of the yield over time and the primary yield. As Geant4-DNA does not have models for argon ions, silicon-28 ions were used instead with the energy modified to match the LET. The silicon ion yields are an approximation of the yields for argon ions, as despite having the same LET there will be a small difference in the radial ionization distribution due to differing Z. Most experimental determinations of G-values for ions of a given LET use LET values that are averaged over the ion track and often include Bragg peak. This is the result of the initial incident energy of the particle used. Only a few measurements of G-values are considered in short track segment LET conditions as the use of sufficiently high ion energies for a slowly changing track segment LET in the measurement volume is required. In the case of averaged LET measurements, the evolution of G-value as function of LET is calculated from averaged values of G by differentiating an empirical function.[27] This method is typically used for measurements of G-values of hydrated electrons, hydroxyl radical, H-atoms, and hydrogen peroxide.[49–54]

The yields of species from irradiation by electrons, protons, alpha particles, carbon ions, and silicon ions of varying energies were modeled using Geant4 to find the effects of the LET of charged particles on the initial and primary yields and the evolution of yields over time for each of the individual species. Further, the hydroxyl radical yield at 100 ns as a function of LET modeled by Geant4 was compared to experimental measurements. The Geant4 yield was normalized to experimental measurements at low LET using a normalization factor calculated using the hydroxyl radical yield at 100 ns from Geant4 simulations of 1 MeV electrons and measurements by Baldacchino et al.[41] The normalization minimizes the effect of the reaction rates and diffusion coefficients allowing testing of the chemistry models' ability to account for the effect of LET on the yield over time.

## 5. RESULTS

### 5.A. Yield verification

For the solvated electron radical shown in Fig. 2, the initial yield in Geant4-DNA is in the middle of the range of yields of both experimental observations and other simulations. At times beyond 1 ns, the yield modeled using Geant4 is 18% higher on average than the yields from experimental measurements and the PARTRAC simulation, while it is only 4% lower on average than the yield modeled by the RITRACKS simulation. The time evolution of the solvated electron yield for Geant4, RITRACKS and the direct pulse experimental observations by Bartels et al.[55] have similar characteristics and only differ greatly in the initial yield.

For the hydroxyl radical yield shown in Fig. 2, the yield modeled by Geant4-DNA chemistry is in good agreement with the yields from PARTRAC, RITRACKS, and experimental measurements up to approximately 1 ns after the physical interactions. For this period, the yield modeled with Geant4 is on average 8% higher than the experimentally observed yields. The yield predicted using Geant4 was subsequently higher than experimental measurements and other simulations up to simulation times of 1 μs. The experimental measurements by Jonah and Miller[56] measured the yield of the hydroxyl radical relative to the yield of the solvated

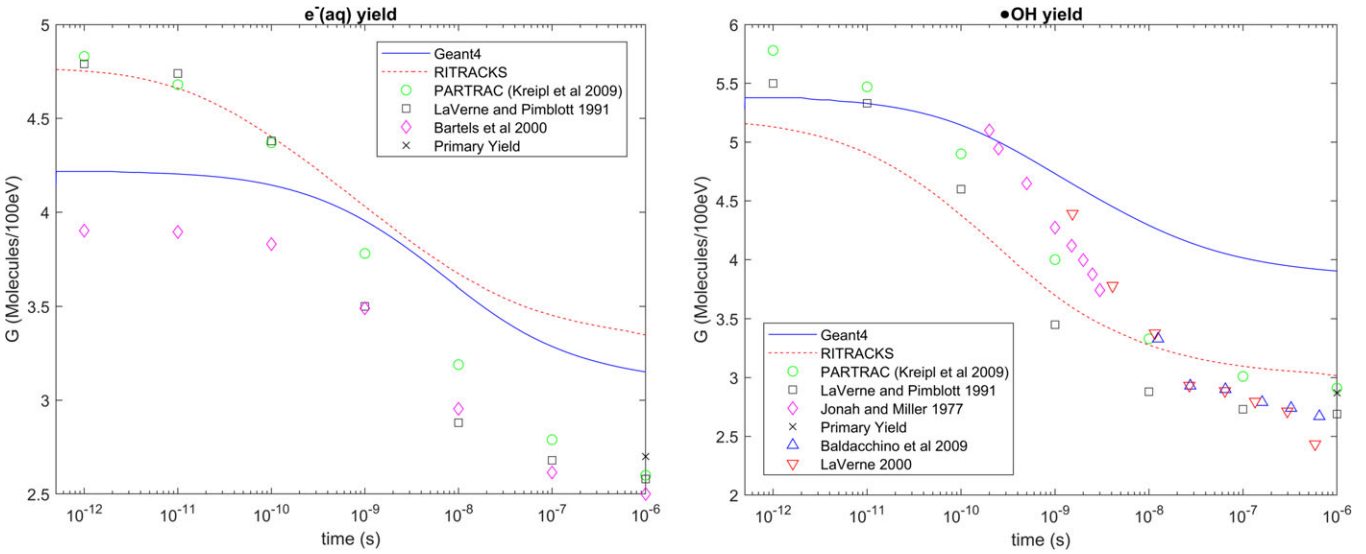


FIG. 2. Yield G (Molecules/100 eV energy deposited) for the solvated electron on the left and hydroxyl radical on the right over time from the Geant4, RITRACKS and PARTRAC[34] simulations for 1 MeV electrons (Geant4 and RITRACKS) and 750 keV electrons (PARTRAC), experimental observations[39,41,55–57] using a fast electron or gamma beam and the low LET primary yield.[5] [Color figure can be viewed at wileyonlinelibrary.com]

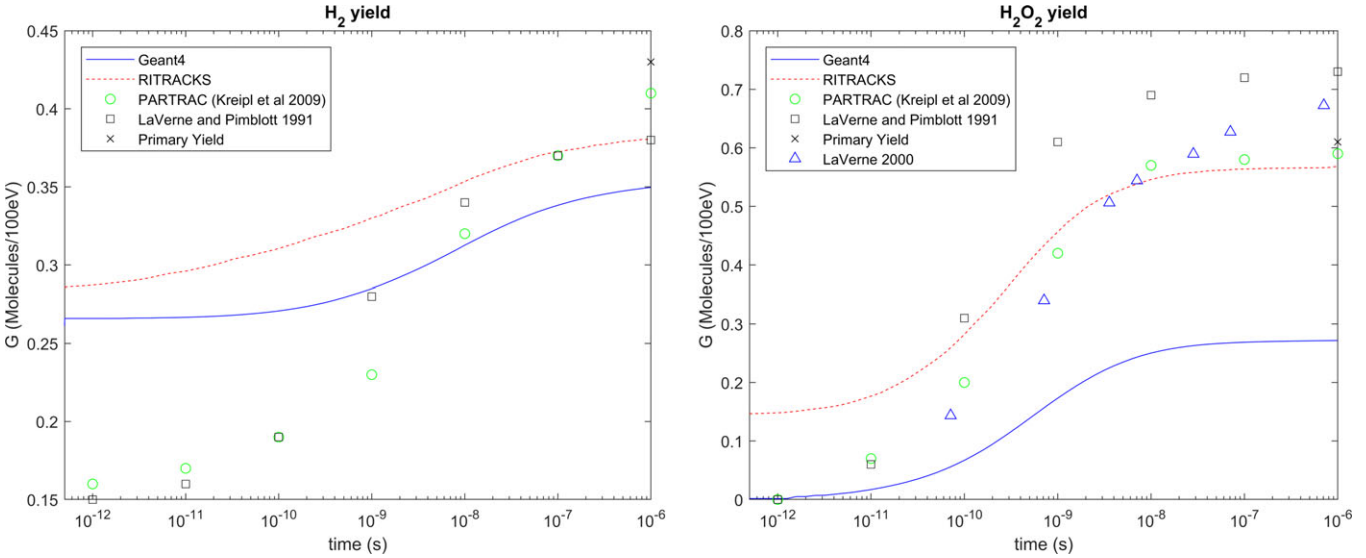


FIG. 3. Yield G (Molecules/100 eV energy deposited) for molecular hydrogen on the left and hydrogen peroxide on the right over time from the Geant4, RITRACKS and PARTRAC[34] simulations for 1 MeV electrons (Geant4 and RITRACKS) and 750 keV electrons (PARTRAC), experimental observations[39,57] using a fast electron or gamma beam and the low LET primary yield.[5] [Color figure can be viewed at wileyonlinelibrary.com]

electron, for the figure their results are used in combination with the solvated electron yield measurement by Bartels et al.[55]

For the molecular hydrogen yield shown in Fig. 3, the yield predicted by Geant4 is on average only 11% lower than the yield predicted using RITRACKS. The initial yield is higher than that modeled by PARTRAC and observed in experimental measurements. The difference in initial yield between Geant4 and RITRACKS compared to PARTRAC is likely due to electron-hole recombination and dissociative attachment processes which are not modeled in PARTRAC. The yield modeled using Geant4 is in reasonable agreement with the yields modeled by RITRACKS and PARTRAC and observed experimentally from 1 ns to 1 μs. Over this period, the Geant4 yield is on average only 8% lower than experimentally observed yields.

The yield of hydrogen peroxide is shown in Fig. 3. Geant4 predicts an initial yield of zero in agreement with PARTRAC and experimental measurements. The yield modeled by Geant4 increases quickly between 10 ps and 10 ns before the growth of the yield slows and the yield becomes almost constant. While this behavior is consistent between RITRACKS, PARTRAC, and experimental data, the growth from 10 ps to

10 ns modeled by Geant4 is considerably lower resulting in a constant hydrogen peroxide yield at 1 μs considerably lower than other simulations and experimental measurements. Note that the chemistry models used in RITRACKS allow ionized and excited water molecules to dissociate, producing primary reactive species, at very short times after physical interactions. This is what causes the yield of a purely secondary reaction product to be non-zero at the start of the chemical stage at 1 ps.

For the hydronium ion shown in Fig. 4, the initial yield modeled using Geant4-DNA chemistry is 11% and 5% lower than the initial yields modeled by PARTRAC and RITRACKS, respectively. While the initial yield differs slightly, the yields over time are very similar for both Geant4 and RITRACKS simulations with the Geant4 yield on average only 2% lower than the RITRACKS yield. The Geant4 yield is in reasonable agreement with experimental observations, especially from 1 to 20 ns; however, the simulated yield falls more slowly than observed in experiments. The Geant4 yield is on average 10% higher than the experimental observations.

For the hydrogen radical shown in Fig. 4, the initial yield modeled using Geant4 is in good agreement with both RITRACKS and PARTRAC. Both Geant4 and RITRACKS simulations show the yield reducing as time after physical interactions increases up to approximately 1 ns before the yields increase again until the end of the simulation. The rate of yield change is greater for RITRACKS than for Geant4; however, the final yields are both in good agreement with the experimentally observed primary yield.[5] The Geant4 yield is only 4% lower than the observed primary yield.

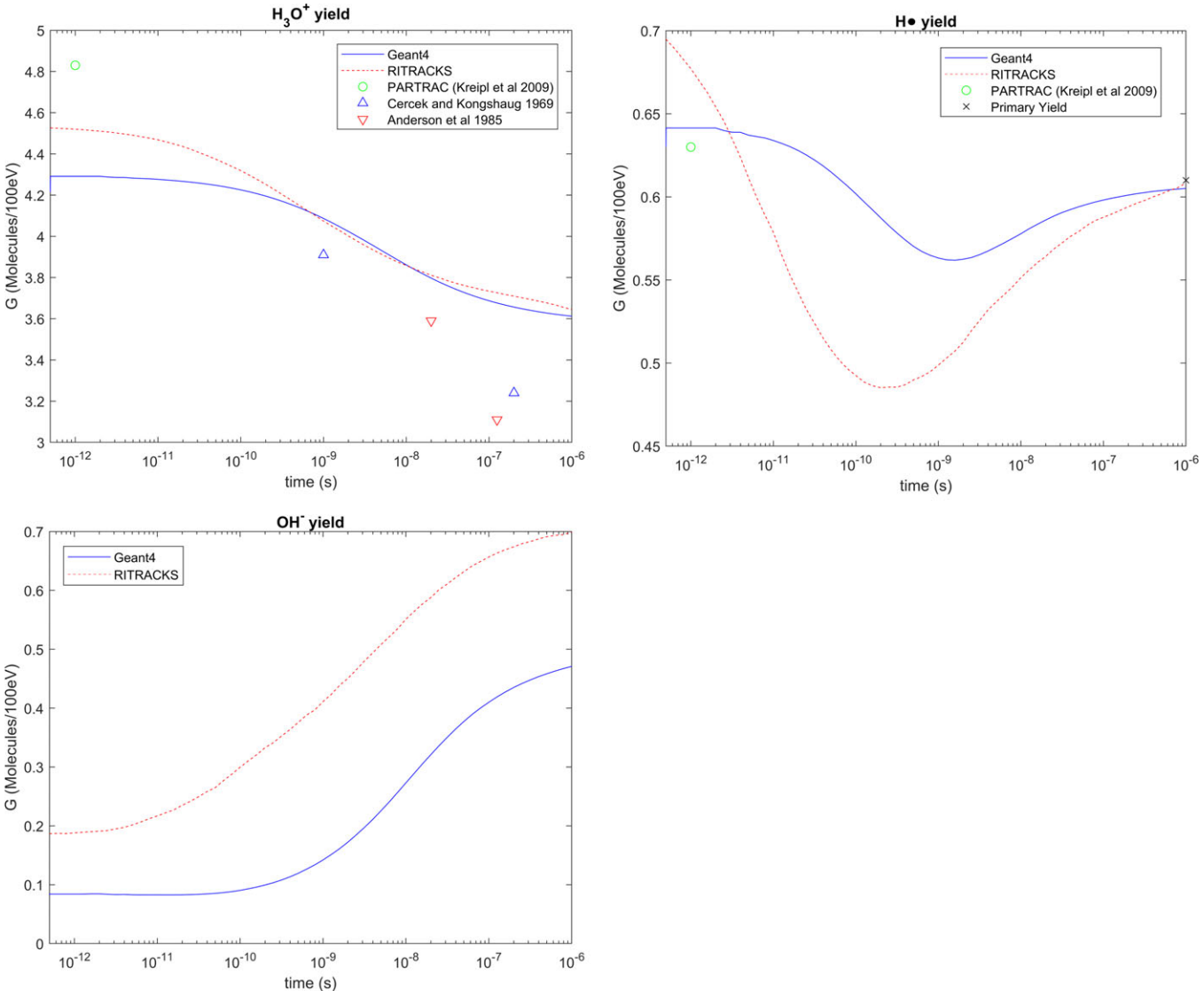


FIG. 4. Yield G (Molecules/100 eV energy deposited) for the hydronium ion on the top left, the hydrogen radical on the right and the hydroxyl ion below over time from the Geant4, RITRACKS and PARTRAC[34] simulations for 1 MeV electrons (Geant4 and RITRACKS) and 750 keV electrons (PARTRAC), experimental observations[58,59] using a fast electron or gamma beam and the low LET primary yield.[5] [Color figure can be viewed at wileyonlinelibrary.com]

As there are no experimental measurements of the hydroxyl ion available, direct validation of the yields from simulations is not currently possible. However, the yields and their trends over time can be compared for the simulations. For the hydroxyl ion yields shown in Fig. 4, the initial yield modeled by Geant4 is approximately half that modeled by RITRACKS; however, given the low yields the absolute difference in initial yield is small. There is a reasonable agreement between the change in yields over time between Geant4 and RITRACKS.

For the solvated electron yields for ions shown in Fig. 5, there is a good agreement between experimental observations between 10 and 100 ns and the Geant4 yield for the carbon ions with the Geant4 yield only 7% lower on average than the experimental observations. For the argon ions, the Geant4 yield is considerably larger than the experimental observations between 2 and 100 ns. This is due to the high dose rate used in the pulse radiolysis experiment resulting in overlapping tracks and accelerated recombination of the solvated electron causing the yield to be underestimated.[61] However, the Geant4 yield is considerably higher at 1 μs than the primary yields. The yields modeled by RITRACKS have a similar behavior over time but have a considerably lower yield which is not consistent with the experimental observations using carbon ions.

For the hydroxyl radical yields for ions shown in Fig. 5, the Geant4 yields for carbon and argon ions have the correct behavior over the 10 ns–1 μs time range for which experimental observations are available; however, they are approximately 65% too high over this time frame. The initial yields modeled by Geant4 are considerably higher than those for RITRACKS; however, the gradient of the earliest experimental observations suggests a higher initial yield than that modeled by RITRACKS.

## 5.B. LET dependence of reactive species yield

For primary reactive species such as the hydroxyl radical, hydronium ion and solvated electrons with yields shown in Figs. 6 and 7, as well as the hydroxyl ion shown in Fig. 7, the initial yield of the species is reduced for radiation with increasing LET. For most secondary reactive species, such as the hydrogen radical, molecular hydrogen and hydrogen peroxide shown in Fig. 8, the initial yield of the species is increased for radiation with higher LET. Additionally, there is a trend across all species that for higher LET radiation types the rate of change in yield over time is increased. As most species' yields are monotonically either decreasing or increasing over time, this increased rate of change results in the difference in yields depending on LET increasing at longer times after the physical interaction. The only exception to this is the hydrogen radical. The nature of this species' yield evolution over time is that the yield first decreases, followed by a smaller increase, meaning that the difference in yield depending on LET actually decreases with time after the physical reactions. The primary yields confirm the observation of yields being lower at 1 μs with increasing LET radiation types for the solvated electron and hydroxyl radical and yields being higher for increasing LET radiation types for the molecular hydrogen and hydrogen peroxide yields.

The primary yield measurements indicate that the reduction in the yield of the solvated electron and growth in the yield of the hydrogen radical should be greater for high LET

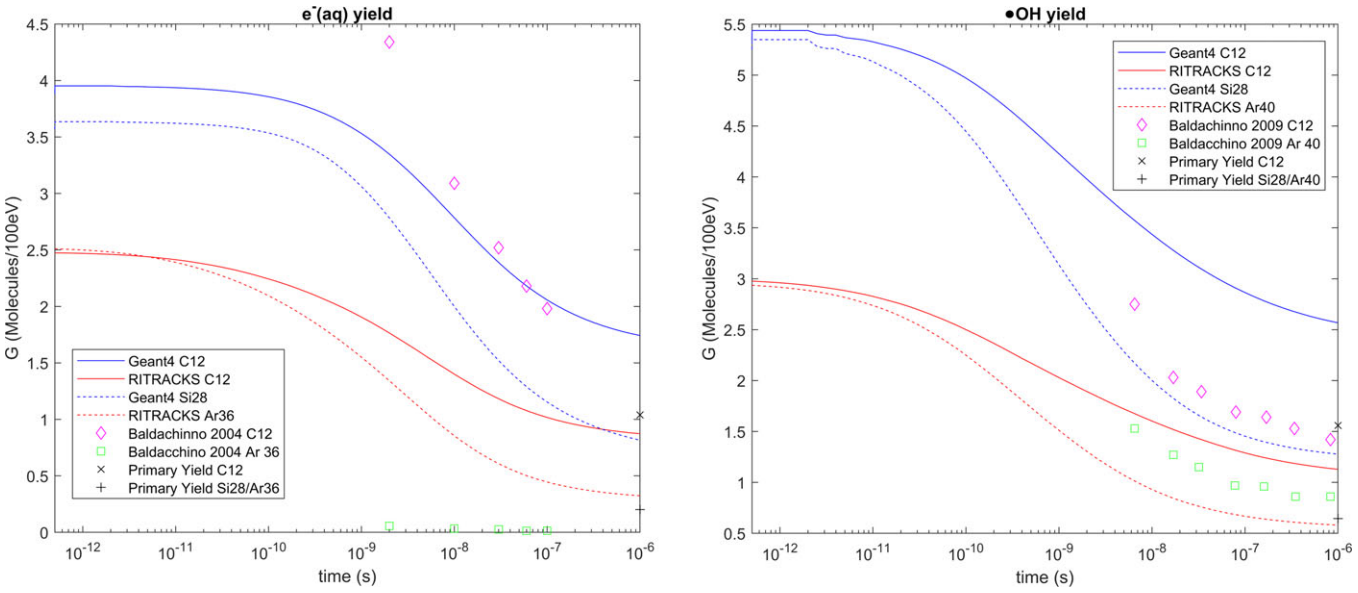


FIG. 5. Yield G (Molecules/100 eV energy deposited) for the solvated electron on the left and hydroxyl radical on the right over time. Yields are shown from Geant4 and RITRACKS simulations of 1.14 GeV carbon-12 ions (Geant4 and RITRACKS), 3.42 GeV argon-36 ions (RITRACKS), and 1.34 GeV silicon-28 ions (Geant4) for the solvated electron and 4.8 GeV carbon-12 ions (Geant4 and RITRACKS), 20 GeV argon-40 ions (RITRACKS) and 5.285 GeV silicon-28 ions (Geant4) for the hydroxy radical. Experimental observations[41,60] of the yield over time using carbon and argon ions and the primary yields[26] are shown. [Color figure can be viewed at wileyonlinelibrary.com]

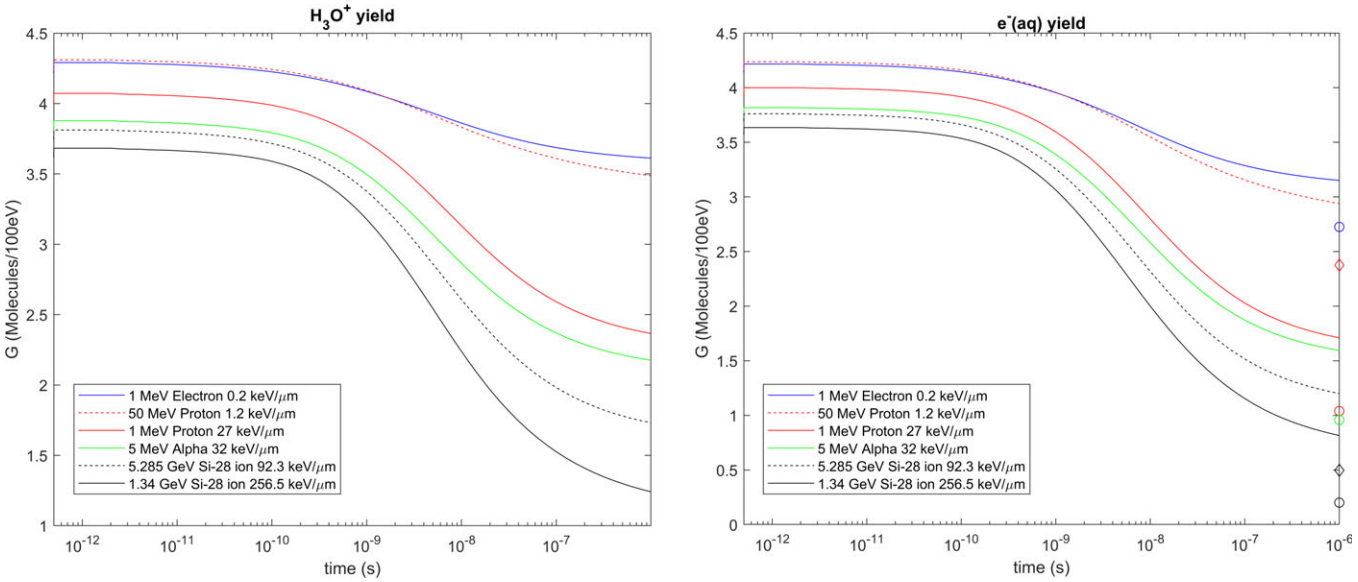


FIG. 6. Yield G (Molecules/100 eV energy deposited) for the hydronium ion on the left and the solvated electron on the right over time from the Geant4 simulation for 1 and 50 MeV protons, 5 MeV alpha particles, 1.34 and 5.285 GeV Si-28 ions and 1 MeV electrons shown by solid red, dashed red, solid green, solid black, dashed black and solid blue lines respectively with primary yields[26] shown by red circle, red diamond, green circle, black circle, black diamond, and blue circle markers, respectively. [Color figure can be viewed at wileyonlinelibrary.com]

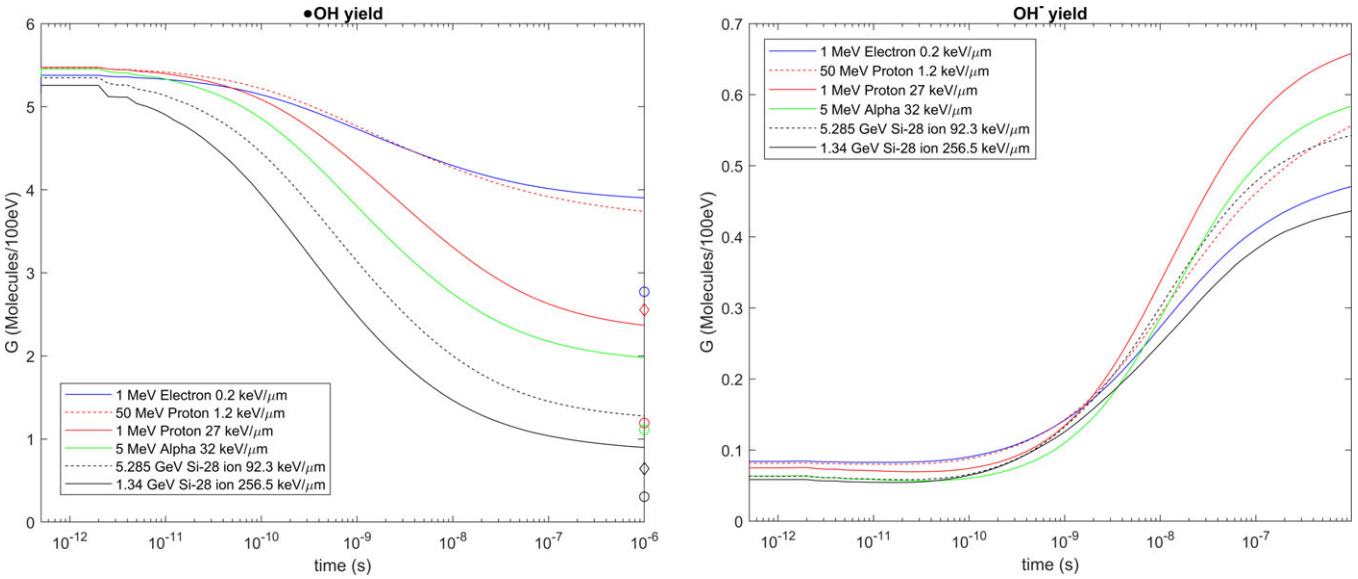


FIG. 7. Yield G (Molecules/100 eV energy deposited) for the hydroxyl radical on the left and the hydroxyl ion on the right over time from the Geant4 simulation for 1 and 50 MeV protons, 5 MeV alpha particles, 1.34 and 5.285 GeV Si-28 ions, and 1 MeV electrons shown by solid red, dashed red, solid green, solid black, dashed black, and solid blue lines respectively with primary yields[26] shown by red circle, red diamond, green circle, black circle, black diamond, and blue circle markers, respectively. [Color figure can be viewed at wileyonlinelibrary.com]

radiation types. Additionally, the measurements indicate that the 1 μs yield of hydrogen peroxide should be lower for higher LET radiation and be higher for lower LET radiation and that the 1 μs yield of the hydrogen radical should decrease with increasing LET.

The hydroxyl radical yield at 100 ns for various radiation types with varying LET is shown in Fig. 9. The Geant4 yields normalized at low LET shows good agreement with experimental measurements. The Geant4 yield of the solvated electron, hydrogen, hydrogen radical, and hydrogen peroxide species at 1 μs for various radiation types with varying LET compared with primary yields[26] is shown in supplementary Figs. S1 and S2.

### 5.C. Completeness of chemical reactions by end of chemistry stage

The number of water molecules that were dissociated and recombined throughout the chemical stage per incident 1 MeV proton modeled using Geant4 is shown in Fig. 10.

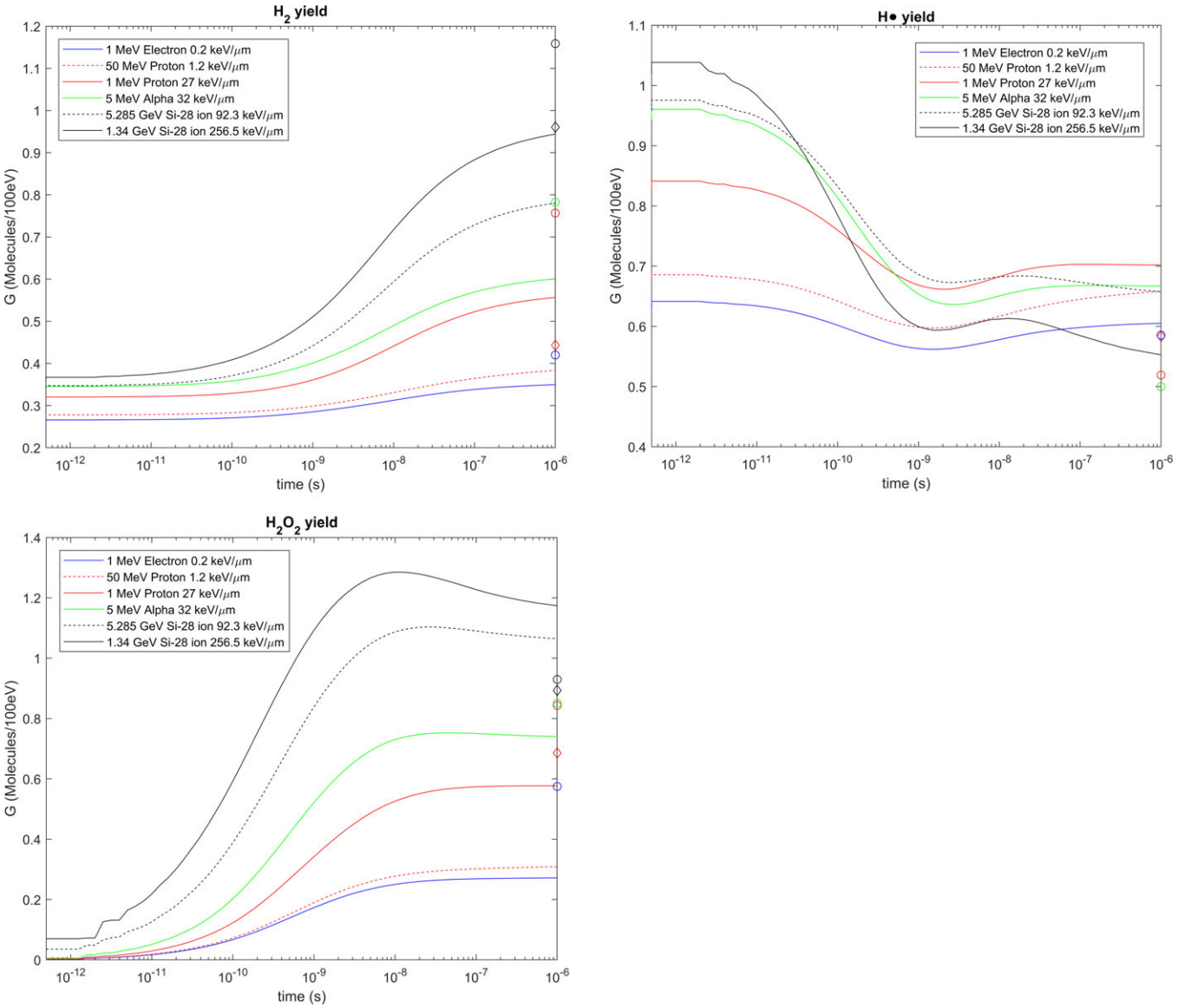


FIG. 8. Yield G (Molecules/100 eV energy deposited) for hydrogen on the top left, the hydrogen radical on the right and hydrogen peroxide on the bottom over time from the Geant4 simulation for 1 and 50 MeV protons, 5 MeV alpha particles, 1.34 and 5.285 GeV Si-28 ions and 1 MeV electrons shown by solid red, dashed red, solid green, solid black, dashed black, and solid blue lines respectively with primary yields[26] shown by red circle, red diamond, green circle, black circle, black diamond, and blue circle markers, respectively. [Color figure can be viewed at wileyonlinelibrary.com]

Almost all of the water molecule dissociation occurs in the physicochemical stage, where ionized and excited water molecules can dissociate prior to the start of recording in the chemistry stage. The number of dissociated water molecules only increases slightly during the chemical stage of the simulation due to a few chemical reactions that result in further dissociation of water molecules. All of the recombination of water molecules occurs in the chemical stage via multiple reactions between species that result in the production of water. The rate of recombination slows greatly at later times in the chemical stage.

The ratio of recombined water molecules to dissociated water molecules during the chemical stage of the simulation is shown in Fig. 10. This ratio represents the completeness of the chemical reactions following radiolysis, that is, the progression to complete recombination of the dissociated water molecules. The recombination fraction is less than 40%, and the rate of the recombination fraction's increase is reduced considerably at later times in the simulation.

## 6. DISCUSSION

### 6.A. Yield verification

In general, there is a good agreement between the yields modeled using Geant4-DNA chemistry and the yields measured experimentally and modeled using other simulation tools. Apart from a few previously noted differences, on average the Geant4 yields are within 20% of available experimental yields and often within 10%. The only major difference is the slow decay of the hydroxyl radical over time and the slow growth of the hydrogen peroxide species over time.

This is problematic as they are important primary and secondary species, respectively. Additionally, the long-lived hydrogen peroxide species can pass through water channels (i.e., aquaporins) in biological membranes and may be responsible for long-range cellular damage. These two differences are likely related to the rate of occurrence of the reaction $^{\bullet}OH + {}^{\bullet}OH \rightarrow H_2O_2$ being too low within the simulation. Another smaller difference is that the yields of the hydronium ion and the solvated electron simulated by Geant4 at 1 μs are higher than the yields measured in experiments. The experimental measurements indicate that the gradient of the change in yields over time of these two species should be slightly increased. This suggests that the rate of occurrence of the reaction $H_3O^+ + e^-_{aq} \rightarrow H^{\bullet} + H_2O$ within the simulation being slightly too low. The rate of occurrence of these reactions can be increased by increasing the reaction rate within the simulation. Care must be taken with any changes not to cause a large disruption of the yields of the other species.

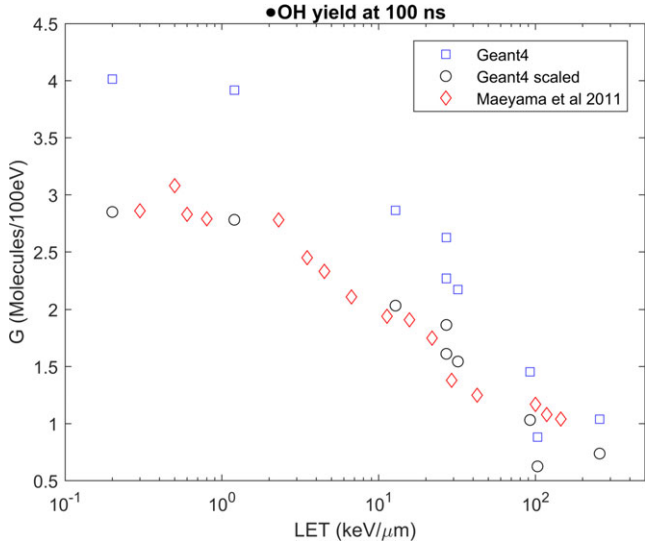


FIG. 9. Yield G (Molecules/100 eV energy deposited) at 100 ns for the hydroxyl radical for radiation types of various LET. Yields from Geant4 (black circles) are normalized to low LET experimental measurements[41] and compared to experimental measurements of the yield for varying LET.[62] [Color figure can be viewed at wileyonlinelibrary.com]

While the direct validation of the hydroxyl ion is impossible without experimental measurements due to the interdependent nature of the chemical reactions being modeled, a reasonable indirect validation can be achieved, as the yield of the hydroxyl ion is closely related to the yields of species that can be directly validated through the dissociation reactions and reactions between species.

## 6.B. LET dependence of reactive species yield

It was found that for radiation with higher LET in general the yields of primary species were decreased while the yields of secondary species increased and that the effect of LET increased with time after physical interactions. These observed effects are likely due to the greater density of ionization events caused by radiation with higher LET. This results in a larger number of reactive species produced in a small volume encompassing the ionization track. As such, the greater density of ionizations for higher LET radiations also results in a higher density of species produced. This increases the probability of reactions between the reactive species, resulting in a decrease in yield for primary species (which are mostly depleted in these reactions) and an increase in yield for secondary species which are mostly created as a result of these reactions.

The hydroxyl radical yield at 100 ns simulated using Geant4 and normalized at low LET agrees with experimental observations for radiation with a range of LETs. This

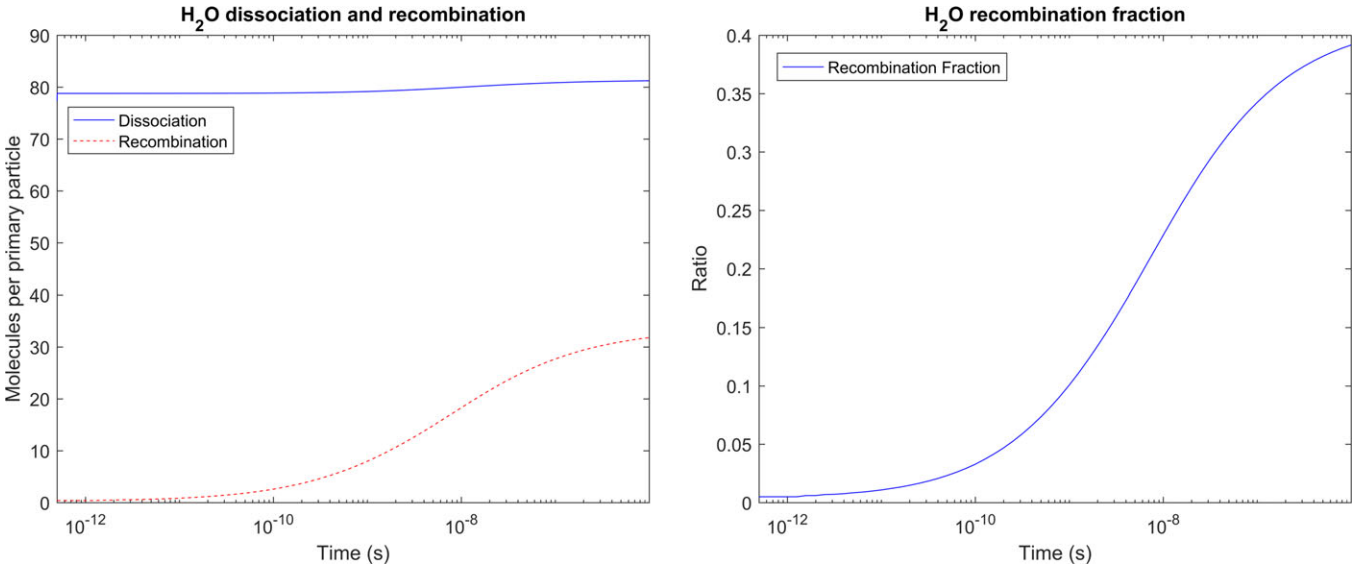


FIG. 10. Left, the number of water molecules per incident proton that undergo dissociation (solid blue line) and recombination (dashed red line) over time. Right, the recombination fraction, the ratio of recombined to dissociated water molecules over time. [Color figure can be viewed at wileyonlinelibrary.com]

indicates that the effect of LET on the radiolysis yields is modeled accurately and hence that Geant4 is homothetically similar to the experimental measurements. However, any inaccuracies at low LET will correspond to inaccuracies at higher LET. The LET determines the density of ionization and excitation events along the simulated track and hence the initial reactive species concentration. As such, the accurate modeling of the effect of LET on yield indicates that the chemistry models accurately account for the effect of initial reactive species concentration on the yields over time. As several different particle types were used over the LET range, there are some large changes in the yield for points with very similar LETs. This is due to radial differences in the ionization due to the different Z of the particles.

### 6.C. Completeness of chemical reactions by end of chemistry stage

Reactive species are mainly produced by radiolysis, the dissociation of water by radiation. After their formation, they react with each other, or water, resulting in the production of secondary species as well as recombining species to form water molecules. As such, the progression of chemical reactions following radiolysis can be measured by tracking the dissociation and recombination of water molecules during the chemical stage. It was found that the dissociation occurs almost entirely before the chemical stage and that recombination occurs throughout the chemical stage of the simulation. The observation that recombination slows toward the end of the chemical stage likely due to diffusion and dilution, and subsequently lower probabilities of reaction.

It was found that the recombination fraction was less than 40% at the end of the chemical stage and that the rate of increase of the recombination fraction was slowing, likely due to the trend for reactive species produced in the same spur to diffuse apart from each other. The recombination fraction of approximately 40% reached at the end of the chemistry stage is consistent with expectations that approximately 40% of initial reactive species will be consumed by spur reactions.[63] The incomplete and slowing recombination indicates that a longer time after the physical interactions than the 1 μs modeled in Geant4 and most other simulations of water radiolysis is required to completely model the chemical reactions following water radiolysis. Due to the intensive computational requirements of extending the detailed modeling for greater periods of time, the results may have to be exported into a chemistry model designed for modeling reactions over a longer time period. Additionally, the slowing rate of recombination indicates that reduced reaction probabilities may promote long-range diffusion of reactive species allowing the exertion of biological damage at relatively distant sites by reactive species that avoid the natural scavenging capacity of the cell (e.g., damage to nuclear DNA from species originating in the cytoplasm).

## 7. CONCLUSION

In this work, we have presented for the first time a comprehensive, independent validation of Geant4-DNA chemical yields in addition to comparison with other radiation chemistry simulations. The yields modeled by Geant4 are in reasonable agreement with available experimental measurements and other simulation models. The only apparent large discrepancies are a slower extinction of the hydroxyl radical yield and a slower formation of the hydrogen peroxide yield over time. This is likely indicative of the reaction between two hydroxyl radicals to form hydrogen peroxide occurring at too low a rate in the simulation. With limited available experimental observations for some of the reactive species modeled, there is a large possible degree of variation of the yields of these species. This uncertainty in the known yields can only be resolved with further experimental observations of water radiolysis and G-value determinations in conditions as near as possible to those used in simulations such as track segment LET, temperature, time resolution, partial pressure of $O_2$, etc.

The investigation of the effect of LET of hadrons on the reactive species yields found that for higher LET, primary species' yields were lower and secondary species' yields were higher. Combined with the observation that these effects were greater for longer times after the physical interactions, it is indicative that the denser ionization events for higher LET radiation result in a higher rate of chemical reactions between the species. Additionally, the effect of LET on the yield was found to be accurately modeled by the simulation. This indicates that validation for lower LET radiation where more data is available should result in the yields modeled by the simulation also being accurate for higher LET radiation.

In Geant4-DNA chemistry simulations, like most radiation chemistry simulations, the modeling of chemical interactions extends to 1 μs after physical interactions. The tracking of the dissociation and recombination of water molecules showed that only 40% of dissociated water molecules had recombined at the end of the chemical stage of the simulation. Additionally, the rate of recombination was slowing. This indicates that a large number of produced reactive species may be long-lived due to reduced reaction probabilities at later times, allowing potential long-range biological effects by reactive species that escape the cell's natural scavenging capacity. To model these effects in addition to those from short lived species, the results from a radiation chemistry simulation may be exported to a simulation designed for longer period modeling of chemical species interactions with a biological target.

The Geant4-DNA chemistry models' simulated yields are in reasonable agreement with experimental observations and other radiation chemistry. The addition of chemistry models to Geant4 allows the modeling of water radiolysis and the 3D distribution of reactive species over time which in combination with Geant4's comprehensive and extensive physics models and potential for complex geometries has great potential utility for many radiobiological simulations.

## ACKNOWLEDGMENTS

The authors thank Ianik Plante for advice in the use of RITRACKS chemistry simulations. We also thank Susanna Guatelli and the Geant4 collaboration for their feedback and advice.

## CONFLICTS OF INTEREST

The authors have no conflicts to disclose.

[a]Author to whom correspondence should be addressed. Electronic mail: eva.bezak@unisa.edu.au.

## REFERENCES

1. Belloni J. Radiation chemistry. Les Ulis, FRANCE: EDP Sciences; 2008. http://ebookcentral.proquest.com/lib/unisa/detail.action?docID=369448.
2. Spinks JWT, Woods RJ. *An Introduction to Radiation Chemistry*, (3rd edn). New York, NY: John Wiley - Interscience; 1990.
3. Hirayama R, Ito A, Tomita M, et al. Contributions of direct and indirect actions in cell killing by high-LET radiations. *Radiat Res*. 2009;171:212–218.
4. Mozumder A. *Fundamentals of Radiation Chemistry*, (1st edn). San Diego, CA: Academic Press; 1999.
5. Farhataziz 1932-, Rodgers MAJ. *Radiation Chemistry : Principles and Applications*. New York, NY: VCH Publishers; 1987. https://inis.iaea.org/search/search.aspx?orig_q=RN:21062396. Accessed July 16, 2018.
6. Kuppermann A. Diffusion Kinetics in Radiation Chemistry: An Assessment. In: Cooper RW, ed. *Physical Mechanisms in Radiation Chemistry*. 1st ed. Washington, DC: US Atomic Energy Commission; 1974:155.
7. Kim J-K, Seo S-J, Kim H-T, et al. Enhanced proton treatment in mouse tumors through proton irradiated nanoradiator effects on metallic nanoparticles. *Phys Med Biol*. 2012;57:8309–8323.
8. Li S, Penninckx S, Karmani L, et al. LET-dependent radiosensitization effects of gold nanoparticles for proton irradiation. *Nanotechnology*. 2016;27:455101.
9. Lin Y, McMahon SJ, Paganetti H, Schuemann J. Biological modeling of gold nanoparticle enhanced radiotherapy for proton therapy. *Phys Med Biol*. 2015;60:4149–4168.
10. Tran HN, Karamitros M, Ivanchenko VN, et al. Geant4 Monte Carlo simulation of absorbed dose and radiolysis yields enhancement from a gold nanoparticle under MeV proton irradiation. *Nucl Instruments Methods Phys Res Sect B*. 2016;373:126–139.
11. Peukert D, Kempson I, Douglass M, Bezak E. Metallic nanoparticle radiosensitisation of ion radiotherapy: a review. *Phys Med*. 2018;47:121–128.
12. Agostinelli S, Allison J, Amako K, et al. GEANT4 - A simulation toolkit. *Nucl Instruments Methods Phys Res Sect A*. 2003;506:250–303.
13. Allison J, Amako K, Apostolakis J, et al. Recent developments in Geant4. *Nucl Instruments Methods Phys Res Sect A*. 2016;835(Suppl C):186–225.
14. Incerti S, Ivanchenko A, Karamitros M, et al. Comparison of GEANT4 very low energy cross section models with experimental data in water. *Med Phys*. 2010;37:4692–4708.
15. Bernal MA, Bordage MC, Brown JMC, et al. Track structure modeling in liquid water: a review of the Geant4-DNA very low energy extension of the Geant4 Monte Carlo simulation toolkit. *Phys Medica*. 2015;31:861–874.
16. Karamitros M, Mantero A, Incerti S, et al. Modeling radiation chemistry in the Geant4 Toolkit. *Prog Nucl Sci Technol*. 2011;2:503–508.
17. Karamitros M, Luan S, Bernal MA, et al. Diffusion-controlled reactions modeling in Geant4-DNA. *J Comput Phys*. 2014;274:841–882.
18. Tachiya M. Theory of diffusion-controlled reactions: formulation of the bulk reaction rate in terms of the pair probability. *Radiat Phys Chem*. 1983;21:167–175.
19. Clifford P, Green NJB, Oldfield MJ, Pilling MJ, Pimblott SM. Stochastic models of multi-species kinetics in radiation-induced spurs. *J Chem Soc Faraday Trans 1 Phys Chem Condens Phases*. 1986;82:2673–2689.
20. Pimblott SM, Pilling MJ, Green NJB. Stochastic models of spur kinetics in water. *Radiat Phys Chem*. 1991;37:377–388.
21. Pimblott SM, Green NJB. Recent advances in the kinetics of radiolytic processes. In: Compton RG, Hancock G, eds. *Research in Chemical Kinetics*. Amsterdam, the Netherlands: Elsevier; 1995:117–174.
22. Green NJB, Pilling MJ, Pimblott SM, Clifford P. Stochastic modeling of fast kinetics in a radiation track. *J Phys Chem*. 1990;94:251–258.
23. Jan S, Santin G, Strul D, et al. GATE: a simulation toolkit for PET and SPECT. *Phys Med Biol*. 2004;49:4543–4561.
24. Perl J, Shin J, Schümann J, Faddegon B, Paganetti H. TOPAS: an innovative proton Monte Carlo platform for research and clinical applications. *Med Phys*. 2012;39:6818–6837.
25. Buxton GV, Greenstock CL, Helman WP, Ross AB. Critical Review of rate constants for reactions of hydrated electrons, hydrogen atoms and hydroxyl radicals (·OH/·O$^-$in Aqueous Solution. *J Phys Chem Ref Data*. 1988;17():513–886.
26. Elliot AJ, Bartels DM. The Reaction Set, Rate Constants and g-Values for the Simulation of the Radiolysis of Light Water over the Range 20 Deg to 350 Deg C Based on Information Available in 2008. 2009. https://inis.iaea.org/search/search.aspx?orig_q=RN:41057263. Accessed July 10, 2018.
27. Hatano Y, Katsumura Y, Mozumder A. *Charged Particle and Photon Interactions With Matter. Recent Advances, Applications, and Interfaces*. 1st ed. Boca Raton, FL: CRC Press; 2010.
28. Kyriakou I, Incerti S, Francis Z. Technical note: improvements in geant 4 energy-loss model and the effect on low-energy electron transport in liquid water. *Med Phys*. 2015;42:3870–3876.
29. Bordage MC, Bordes J, Edel S, et al. Implementation of new physics models for low energy electrons in liquid water in Geant4-DNA. *Phys Medica*. 2016;32:1833–1840.
30. Incerti S, Kyriakou I, Bernal MA, et al. Geant4-DNA example applications for track structure simulations in liquid water: a report from the Geant4-DNA Project. *Med Phys*. 2018;45:e722–e739.
31. Terrissol M, Beaudre A. Simulation of space and time evolution of radiolytic species induced by electrons in water. *Radiat Prot Dosimetry*. 1990;31:175–177.
32. Meesungnoen J, Jay-Gerin J-P, Filali-Mouhim A, Mankhetkorn S. Low-energy electron penetration range in liquid water. *Radiat Res*. 2002;158:657–660.
33. Ritchie RH, Hamm RN, Turner JE, Bolch WE. Interactions of low-energy electrons with condensed matter: relevance for track structure. In: Varma MN, Chatterjee A, eds. *Computational Approaches in Molecular Radiation Biology: Monte Carlo Methods*. Boston, MA: Springer US; 1994:33–47.
34. Kreipl MS, Friedland W, Paretzke HG. Time- and space-resolved Monte Carlo study of water radiolysis for photon, electron and ion irradiation. *Radiat Environ Biophys*. 2009;48:11–20.
35. Buxton GV. Radiation chemistry of the liquid state. In: Farhataziz 1932-, Rodgers MAJ, eds. *Radiation Chemistry : Principles and Applications*. New York, NY: VCH Publishers; 1987:321–350.
36. Incerti S, Douglass M, Penfold S, Guatelli S, Bezak E. Review of Geant4-DNA applications for micro and nanoscale simulations. *Phys Medica*. 2016;32:1187–1200.
37. Abolfath RM, Carlson DJ, Chen ZJ, Nath R. A molecular dynamics simulation of DNA damage induction by ionizing radiation. *Phys Med Biol*. 2013;58:7143–7157.
38. Pachnerová Brabcová K, Štěpán V, Karamitros M, et al. Contribution of indirect effects to clustered damage in DNA irradiated with protons. *Radiat Prot Dosimetry*. 2015;166:44–48.
39. LaVerne JA, Pimblott SM. Scavenger and time dependences of radicals and molecular products in the electron radiolysis of water: examination of experiments and models. *J Phys Chem*. 1991;95:3196–3206.
40. Pimblott SM, La Verne JA. Scavenger concentration dependences of yields in radiation chemistry. *J Phys Chem*. 1992;96:746–752.
41. Baldacchino G, Maeyama T, Yamashita S, et al. Determination of the time-dependent OH-yield by using a fluorescent probe. Application to heavy ion irradiation. *Chem Phys Lett* 2009;6:275–279.

42. Belov OV, Batmunkh M, Incerti S, Lkhagva O. Radiation damage to neuronal cells: simulating the energy deposition and water radiolysis in a small neural network. *Phys Medica*. 2016;32:1510–1520.
43. Tian Z, Jiang SB, Jia X. Accelerated Monte Carlo simulation on the chemical stage in water radiolysis using GPU. *Phys Med Biol*. 2017;62:3081–3096.
44. Plante I, Cucinotta FA. Ionization and excitation cross sections for the interaction of HZE particles in liquid water and application to Monte Carlo simulation of radiation tracks. *New J Phys*. 2008;10:125020.
45. Plante L, Cucinotta FA. Cross sections for the interactions of 1 eV-100 MeV electrons in liquid water and application to Monte-Carlo simulation of HZE radiation tracks. *New J Phys*. 2009;11:063047.
46. Friedland W, Dingfelder M, Kundrát P, Jacob P. Track structures, DNA targets and radiation effects in the biophysical Monte Carlo simulation code PARTRAC. *Mutat Res - Fundam Mol Mech Mutagen*. 2011;711:28–40.
47. Douglass M, Penfold S, Bezak E. Preliminary Investigation of Microdosimetric Track Structure Physics Models in Geant4-DNA and RITRACKS. *Comput Math Methods Med*. 2015;2015:968429.
48. Klassen NV. Primary products in radiation chemistry. In: Farhataziz 1932-, Rodgers MAJ, eds. *Radiation Chemistry : Principles and Applications*. New York, NY: VCH Publishers; 1987:29–64.
49. Iwamatsu K, Sundin S, LaVerne JA. Hydrogen peroxide kinetics in water radiolysis. *Radiat Phys Chem*. October 2017;2018:207–212.
50. Wasselin-Trupin V, Baldacchino G, Bouffard S, Hickel B. Hydrogen peroxide yields in water radiolysis by high-energy ion beams at constant LET. *Radiat Phys Chem*. 2002;65:53–61.
51. Crumière F, Vandenborre J, Blain G, Haddad F, Fattahi M. Evolution of heavy ions (He2 + , H+) radiolytic yield of molecular hydrogen vs. "Track-Segment" LET values. *Radiochim Acta* 2017;105:487–492.
52. Huerta Parajon M, Rajesh P, Mu T, Pimblott SM, LaVerne JA. H atom yields in the radiolysis of water. *Radiat Phys Chem*. 2008;77:1203–1207.
53. Pimblott SM, Laverne JA, Barteis DM, Jonah CD. Reconciliation of transient absorption and chemically scavenged yields of the hydrated electron in radiolysis. *J Phys Chem*. 1996;100:9412–9415.
54. Sanguanmith S, Meesungnoen J, Jay-Gerin JP. Time-dependent yield of OH radicals in the low linear energy transfer radiolysis of water between 25 and 350 & #xB0;C. *Chem Phys Lett*. 2013;588:82–86.
55. Bartels DM, Cook AR, Mudaliar M, Jonah CD. Spur decay of the solvated electron in picosecond radiolysis measured with time-correlated absorption spectroscopy. *J Phys Chem A*. 2000;104:1686–1691.
56. Jonah CD, Miller JR. Yield and decay of the OH radical from 200 ps to 3 ns. *J Phys Chem*. 1977;81:1974–1976.
57. LaVerne JA. OH radicals and oxidizing products in the gamma radiolysis of water. *Radiat Res*. 2000;153:196–200.
58. Cercek B, Kongshaug M. Hydrogen ion yields in the radiolysis of neutral aqueous solutions. *J Phys Chem*. 1969;73:2056–2058.
59. Anderson RF, Vojnovic B, Michael BD. The radiation-chemical yields of H3O+ and OH- as determined by nanosecond conductimetric measurements. *Radiat Phys Chem*. 1985;26:301–303.
60. Baldacchino G, Vigneron G, Renault J-P, et al. A nanosecond pulse radiolysis study of the hydrated electron with high energy ions with a narrow velocity distribution. *Chem Phys Lett*. 2004;385:66–71.
61. Kreipl MS, Friedland W, Paretzke HG. Interaction of ion tracks in spatial and temporal proximity. *Radiat Environ Biophys*. 2009;48:349–359.
62. Maeyama T, Yamashita S, Baldacchino G, et al. Production of a fluorescence probe in ion-beam radiolysis of aqueous coumarin-3-carboxylic acid solution-1: beam quality and concentration dependences. *Radiat Phys Chem*. 2011;80:535–539.
63. Buxton GV. An overview of the radiation chemistry of liquids. In: Belloni J, ed. *Radiation Chemistry: From Basics to Applications in Material and Life Sciences*. Les Ulis, FRANCE: EDP Sciences; 2008:3–16.

## SUPPORTING INFORMATION

Additional supporting information may be found online in the Supporting Information section at the end of the article.

**Figure S1:** Yield G (Molecules/100 eV energy deposited) at 1 μs for the solvated electron on the left and hydrogen on the right for radiation types of various LET. Yields from Geant4 (blue squares) are compared to experimentally derived values of the primary yield for varying LET.[26]

**Figure S2:** Yield G (Molecules/100 eV energy deposited) at 1 μs for hydrogen peroxide on the left and the hydrogen radical on the right for radiation types of various LET. Yields from Geant4 (blue squares) are compared to experimentally derived values of the primary yield for varying LET.[26]